

# Procedures to Build Trust in Nonlinear Elastoplastic Integration Algorithm: Solution and Code Verification

Yuan Feng<sup>1</sup> · Kaveh Zamani<sup>2</sup> · Han  
Yang<sup>1</sup> · Hexiang Wang<sup>1</sup> · Fangbo Wang<sup>1</sup> ·  
Boris Jeremić<sup>1,3</sup>

Received: date / Accepted: date  
(The correct dates will be entered by the editor)

version: 18. December, 2018 15:43

---

Professor Boris Jeremić E-mail: jeremic@ucdavis.edu

1

Department of Civil and Environmental Engineering, University of California, Davis, California, U.S.A.

2

Senior Flood Modeler, Wood Rodgers, Sacramento, California, U.S.A.

3

Earth and Environmental Sciences Area, Lawrence Berkeley National Laboratory, Berkeley, California, U.S.A.

## Contents

1	Introduction . . . . .	3
2	Background . . . . .	4
3	Elastoplastic Constitutive Integration Algorithm . . . . .	6
3.1	Explicit, Forward Euler Algorithm . . . . .	6
3.2	Implicit, Backward Euler Algorithm . . . . .	7
4	Theoretical Basis for Verification . . . . .	8
4.1	The Asymptotic Regime of Convergence . . . . .	8
4.2	Richardson Extrapolation Technique as a Verification Tool . . . . .	8
4.3	Uncertainties in Numerical Simulation . . . . .	9
4.4	Grid Convergence Index . . . . .	10
4.5	Accuracy order of Elastoplastic Algorithm . . . . .	11
4.5.1	Analytical Determination of Accuracy Order . . . . .	11
4.5.2	Numerical Estimation of Accuracy Order . . . . .	11
5	Elastoplastic Material Models . . . . .	12
5.1	The von-Mises Yield Surface . . . . .	13
5.2	Hyperbolic Drucker-Prager Yield Surface . . . . .	13
5.3	Non-associative Plastic Flow . . . . .	14
5.4	Armstrong-Frederick Hardening Law . . . . .	14
6	Error Maps for Elastoplastic Constitutive Integration . . . . .	14
6.1	Error Map for von-Mises Perfectly Plastic Material Model . . . . .	15
6.2	Error Map for Hyperbolic Drucker-Prager Linear Kinematic Hardening Material Model . . . . .	17
6.3	Error Map for Hyperbolic Drucker-Prager Armstrong-Frederick Nonlinear Kinematic Hardening Material Model . . . . .	19
6.4	Numerical Accuracy Estimation for Associated Drucker-Prager Linear Kinematic Hardening Material Model . . . . .	21
6.5	Numerical Accuracy Estimation for Non-Associated Drucker-Prager Nonlinear Kinematic Hardening Material Model . . . . .	22
7	Conclusion and Final Remarks . . . . .	24

**Abstract** In the last decades, with the development of a number of nonlinear elastic-plastic integration algorithms, the correctness or accuracy of the underlying solution becomes the main concern, in both academia and industry. Correctness or accuracy can be estimated (and improved) using verification. Verification is one of the main procedures to build trust in the numerical modeling of any phenomena. A full verification process comprises (a) solution verification (calculation verification) and (b) code verification.

Presented in this paper are verification procedures for constitutive, elastic-plastic integration algorithms, as used in computational nonlinear solid mechanics. Both explicit and implicit integration algorithms for elastic-plastic constitutive equations are verified using existing and developed new verification technique. Verification techniques used include prescribed solution forcing (PSF) and Richardson extrapolation (RE). In addition, grid convergence index (GCI) is applied to estimate the algorithmic uncertainty during the integration process.

Verification of elastic-plastic integration algorithms is applied to a number of material models: from simple von-Mises perfectly plastic to sophisticated hyperbolic Drucker-Prager with nonlinear Armstrong-Frederick rotational kinematic hardening. Besides, algorithmic uncertainty is estimated with both associative and non-associative material model. In addition caveats and pitfalls to consider in the code/solution verification processes are deeply discussed.

**Keywords** Elastoplastic Algorithms · Prescribed Solution Forcing · Richardson Extrapolation · Grid Convergence Index (GCI)

## 1 Introduction

Modern computational modeling systems are very often used in engineering community for design and assessment. Given all the positive aspects of using computational modeling systems, a fundamental question is this: to what extent can we trust model results (Oberkampf et al., 2002b; Roy and Oberkampf, 2011). There are a number of engineering failures that can be tied to problems in the numerical codes (Jazequel and Meyer, 1997; Grottke and Trivedi, 2007) or to misuse of models. The set of activities and procedures that can be used to build trust in numerical modeling results are called verification and validation (Wise et al., 2013; Roy and Oberkampf, 2011). According to Roache's definition (Roache, 1998b) verification is the response to the following question: "Is the model solving mathematical equations correctly?". On the other hand, validation can be defined through this question: "Is the model solving the correct equations?" (Oberkampf et al., 2002b; Roy and Oberkampf, 2011). Focus of this paper is on verification of numerical algorithms to integrate elastic-plastic constitutive equations. Validation of elastic-plastic models is not within current scope of this paper and is left for future publications.

A general elastic-plastic constitutive model usually consist of four components:

1. *Elastic law*, that controls elastic response before solid plastifies. Elastic model/law response can be linear or nonlinear.
2. *Yield criterion (function)* that separates elastic from elastic-plastic region. Yield function is a function of the state of stress and a set of internal variables. The common yield criteria can be pressure independent (such as von

Mises and Tresca) or pressure dependent (Mohr-Coulomb or Drucker-Prager) (Drucker and Prager, 1952). In addition to the common yield criterion, a hyperbolic yield surface is usually used to smooth the apex for higher order derivation. Abbo and Sloan (1995) used this approach for Mohr-Coulomb.

3. *Plastic flow directions*, that prescribe direction of plastic deformation once material plastifies. Plastic flow directions are a function of the state of stress and a set of internal variables. Plastic flow direction can be associated with the yield function (plastic flow is parallel to the normal to the yield function/surface (usually for metals) or non-associated, when plastic flow directions are not normal to yield function/surface (usually for geomaterials)).
4. *Hardening laws* that controls evolution of internal variables. Hardening laws can control evolution of scalar internal variables (isotropic hardening/softening (Muir Wood, 1990)), second order tensors (kinematic hardening (Armstrong and Frederick, 1966)) and fourth order tensor (distortional hardening (Baltov and Sawczuk, 1965)).

The four components, using different elastic laws, yield functions, plastic flow directions and hardening laws, can be combined to develop a number of elastic-plastic material models. In this paper two models are used for verification, namely, von Mises and hyperbolic Drucker-Prager elastic-plastic material model, both with linear and nonlinear hardening laws. Hyperbolic Drucker-Prager used here is developed based on the idea from Abbo and Sloan (1995).

General numerical integration algorithms for elastic-plastic constitutive equations are state-updating procedure. Commonly used are explicit (forward Euler) and implicit (backward Euler) elastic-plastic integrations algorithms.

The paper is structured as follows. Section 2 introduces the history of verification from computational fluid dynamics to nonlinear finite element analysis of solid mechanics. Section 3 shortly introduces the elastic-plastic algorithms. Section 4 presents the theoretical basis of the applied verification techniques. Section 5 briefly reviewed the verified elastic-plastic material model. Section 6 shows the verification examples of different elastic-plastic material models.

## 2 Background

Computer speed is increasing at a steady pace, following Moore's observation, that is sometimes called Moore's law (Moore, 1965) that states that "The number of transistors in a dense integrated circuit doubles approximately every two years", leading to ever faster computers. In addition, software developments, in last number of decades, have made it possible to develop very sophisticated mechanics designs for a large number (almost all) of recent civil engineering objects. Use of computational modeling in the area of mechanics in other fields of engineering is also noted, particularly in mechanical, aerospace and biomedical engineering. It is also worth noting Wirth's law (Wirth, 1995), that states that "Software is getting slower more rapidly than hardware is getting faster", is almost balancing hardware speed advancements. Nevertheless, sophistication in modeling capabilities in computational mechanics (and other fields of computational modeling) is bringing forward significant number of advantages, with economy and safety being the main beneficiaries.

Despite significant advances in modeling and simulations, there exists a number of cases where (problematic) results from nonlinear analysis contributed to engineering incidents or even failures (Hatton and Roberts, 1994; Hatton, 1997; Selby et al., 1997).

The main question that is frequently asked, particularly for nonlinear analysis results, is this: "how much can we trust results of the numerical analysis for use in design and assessment of infrastructure objects?". This question can be split in two questions:

1. How much can (should) we trust model implementations?
2. How much can (should) we trust mathematical models?

Answer to both questions can be found out through a process of verification (question #1) and validation (question #2). Field of the Verification and Validation (V&V) has received significant interest in view of ever growing use of numerical modeling in design and assessment (Roache, 1998a; Oberkampf et al., 2002b; Roy and Oberkampf, 2011; Oden et al., 2005; Babuška and Oden, 2004; Oden et al., 2010a,b).

V&V provide a rigorous framework to assessing the accuracy computational simulations. Verification has two parts: code verification and solution verification. Code verification (solver verification) is a procedure to ensure that a code is bug free. Code verification is a one-time task and it should be only repeated when the source code is modified. Solution verification is a procedure to check if the simulation results are accurate.

The simulation verification techniques were developed primarily by the U.S. Department of Energy (DOE) after adaptation of Comprehensive Nuclear-Test-Ban Treaty (CTBT) in 1996 (Oberkampf and Roy, 2010). Both code verification and calculation verification studies are based on mesh convergence test. In this test, behavior of numerical error is studied as mesh size shrinks. There are a number of methods to perform mesh convergence test: and Richardson Extrapolation (Roache and Knupp, 1993), Method of Manufactured Solution (MMS) (Roache, 2002) and Method of Exact solutions (MES) (Zamani et al., 2014). Other methods of code/solution verification were suggested in the literature in order to overcome practical difficulties or shortcomings of the above mentioned methods: Prescribed Solution Forcing Method (Dee, 1991), Method of Nearby Solution (Roy et al., 2007), and External Verification Analysis (Ingraham and Hixon, 2013). It is worth mentioning that there is no consensus on the naming of verification methods in the verification literature, so different names will be used, for, potentially similar procedures, and full reference will be provided to original development.

Application of numerical verification techniques started in computational fluid mechanics and eventually founds its way into computational solid mechanics (Kamojjala et al., 2013). Although the fundamental concepts are similar, there are inherent differences in implementation of the verification methods. To the best of the authors' knowledge, full implementation of numerical verification test in computational geomechanics is scarce (Sjögreen and Petersson, 2011). Described in this paper are code and solution verification techniques for elastic-plastic constitutive integration algorithms. Additionally, implemented and described is Roache Grid Convergence Index (Roache, 1997) test to uncover numerical uncertainty in the elastic-plastic simulations.

### 3 Elastoplastic Constitutive Integration Algorithm

Elastoplastic integration algorithm is used to solve for the stress increment from a strain increment. The elastic-plastic integration algorithm is a two-step algorithm including the elastic predictor and plastic corrector (Crisfield, 1991). The elastic predictor step is similar for different algorithms. Depending on the direction of the plastic corrector, the elastic-plastic algorithms are generally divided into explicit, forward Euler and implicit, backward Euler algorithms. Both explicit and implicit algorithms are special cases of a general mid-point algorithm (Ortiz and Popov, 1985; Crisfield, 1991, 1997). These two constitutive algorithms represent the most common constitutive integration algorithms. Explicit algorithm uses the starting elastic-plastic point to define the direction of the plastic corrector. Implicit algorithm uses the final stress state to define the direction of the plastic corrector. Iterations are required for the implicit algorithm in order to find the final stress state.

Small deformation, incremental elasto-plastic equations (1), given below:

$$\begin{aligned}
 d\sigma_{ij} &= E_{ijkl} (d\epsilon_{kl} - d\epsilon_{kl}^{pl}) \\
 d\epsilon_{ij}^{pl} &= d\lambda m_{ij}(\sigma, q_*) \\
 dq_* &= d\lambda h_*(\sigma, q_*) \\
 F(\sigma, q_*) &= 0 \wedge dF(\sigma, q_*) = 0
 \end{aligned} \tag{1}$$

are used to solve for an increment of stress ( $d\sigma_{ij}$ ), an increment of internal variables ( $dq_*$ ) and for elastic-plastic stiffness tensor ( $E_{ijkl}^{el-pl}$ ) at a material point (integration point, Gauss point) for a given increment in strain ( $d\epsilon_{kl}$ ). Small deformation assumption is used so that an increment of strain ( $d\epsilon_{ij}$ ) can be defined from increments in displacements ( $du_i$ ) as  $d\epsilon_{ij} = 1/2(du_{i,j} + du_{j,i})$ . Small deformation assumption allows for additive split of strain increment into elastic and plastic parts ( $d\epsilon_{kl} = d\epsilon_{kl}^{el} + d\epsilon_{kl}^{pl}$ ). Internal variables ( $q_*$ ) can be (a) scalars, for isotropic hardening/softening, (b) second-order tensors, for kinematic hardening/softening or (c) fourth order tensors, for distortional hardening/softening. The scalar  $d\lambda$  is the plastic multiplier. Plastic flow directions are defined by the tensor  $m_{ij}$ , and hardening/softening rule is defined by the tensor function  $h_*(\sigma, q_*)$ . The yield function  $F(\sigma, q_*)$  separates elastic response of material for ( $F(\sigma, q_*) < 0$ ) from elastic-plastic response of material ( $F(\sigma, q_*) = 0$ ). It is important to note that yield function  $F$  cannot be larger than zero  $F(\sigma, q_*) \not> 0$ , hence  $dF(\sigma, q_*) = 0$ . Numerically, this requirement of non-positive yield function ( $dF(\sigma, q_*) \not> 0$ ) cannot be enforced for explicit integration algorithm, as there are no equilibrium iterations, and the stress solution in general drifts away from the yield surface into plastic region.

#### 3.1 Explicit, Forward Euler Algorithm

An explicit, forward Euler algorithm uses plastic flow directions and hardening/softening function at the initial elastic-plastic state, that is on the yield surface, to calculate the increment in stress ( $d\sigma_{ij}$ ) and continuum, tangent elastic-plastic

stiffness tensor  ${}^{cont}E_{ijkl}^{ep}$  (Crisfield, 1991, 1997; Chen, 1994). The plastic-multiplier  $d\lambda$  is solved for as

$$d\lambda = \frac{{}^{cross}n_{ij}E_{ijkl}d\epsilon_{kl}}{{}^{cross}n_{ab}E_{abcd}{}^{cross}m_{cd} - {}^{cross}\xi_*h_*} \quad (2)$$

where the tensor  ${}^{cross}n_{ij} = \partial F / \partial \sigma_{ij}$  is the normal to the yield surface at the starting point, while the parameter  ${}^{cross}\xi_* = \partial F / \partial q_*$  is the derivative with respect to the corresponding internal variables, both for a stress – internal variable state on the yield surface, Continuum, tangent stiffness tensor is obtained as

$${}^{cont}E_{ijkl}^{ep} = E_{ijkl} - \frac{E_{ijab}{}^{cross}m_{ab}{}^{cross}n_{cd}E_{cdkl}}{{}^{cross}n_{ot}E_{otrs}{}^{cross}m_{rs} - \xi_*h_*} \quad (3)$$

### 3.2 Implicit, Backward Euler Algorithm

An implicit, backward Euler algorithm uses state of stress and internal variables at the final step (solution) of particular increment to develop the consistent, algorithmic stiffness tensor  ${}^{cons}E_{ijkl}^{ep}$  (Simo and Taylor, 1985; Runesson and Samuelsson, 1985). Since the state of stress  $\sigma_{ij}$  and internal variables  $q_*$  at the final, solution state is not known before the calculation, the implicit algorithm requires iterations to converge to the final results.

In the implicit algorithm, the plastic-multiplier  $d\lambda$  is iteratively solved for (Jeremić, 1994) as

$$d\lambda = \frac{{}^{next}F - {}^{next}n_{kl}r_{ij}{}^{next}T_{ijkl}^{-1}}{{}^{next}n_{ot}E_{abcd}{}^{next}H_{cd}{}^{next}T_{abot}^{-1} - \xi_*h_*} \quad (4)$$

where  $r_{ij} = \sigma_{ij} - ({}^{pred}\sigma_{ij} - \lambda E_{ijkl}m_{kl})$  is the stress residual from the last iteration, and the tensors  $T_{ijkl}$  and  $H_{ij}$  are given as

$$\begin{aligned} T_{ijkl} &= \delta_{ik}\delta_{jl} + \lambda E_{ijab} \frac{\partial m_{ab}}{\partial \sigma_{kl}} \\ H_{ij} &= m_{ij} + \lambda \frac{\partial m_{ij}}{\partial q_*} h_* \end{aligned} \quad (5)$$

Iterations continue until predetermined tolerance for the stress residual ( $r_{ij}$ ) and the yield function ( $F$ ) are reached.

The consistent<sup>1</sup>, algorithmic elastic-plastic stiffness tensor is then obtained as

$${}^{cons}E_{ijkl}^{ep} = E_{ijkl} - \frac{R_{ijab}{}^{next}H_{ab}{}^{next}n_{cd}R_{cdkl}}{{}^{next}n_{ot}R_{otrs}{}^{next}H_{rs} - \xi_*h_*} \quad (6)$$

where the tensors  $R_{ijab}$ ,  $T_{ijmn}$ , and  ${}^{n+1}H_{kl}$  are defined as

$$\begin{aligned} R_{ijab} &= T_{ijkl}^{-1} E_{klab} \\ T_{ijmn} &= \delta_{im}\delta_{nj} + d\lambda E_{ijkl} \frac{\partial m_{kl}}{\partial \sigma_{mn}} \Big|_{n+1} \\ {}^{n+1}H_{kl} &= {}^{n+1}m_{kl} + \frac{\partial m_{kl}}{\partial q_*} \Big|_{n+1} h_* \end{aligned}$$

<sup>1</sup> Consistent with the Newton iterative algorithm on global, finite element level.

## 4 Theoretical Basis for Verification

### 4.1 The Asymptotic Regime of Convergence

For numerical solutions that rely on discretization in space or in time, mesh size or time step size choice is crucial for accuracy of the solution. When the mesh size or step size  $\Delta x$  is large, the error oscillates since the discretization size is too large to represent the actual continua (space or time) in the discretized domain. As mesh size – step size ( $\Delta x$ ) is reduced to the middle size region, the error starts to decrease asymptotically. This region is called the asymptotic regime of convergence. However, as the mesh size – step size ( $\Delta x$ ) is reduced even further, the round-off error contributes to a rapid increase in solution error. This is illustrated in Figure 1.

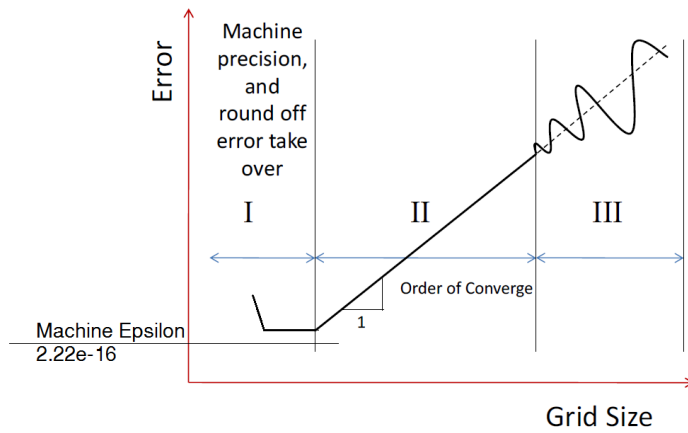


Fig. 1: Behavior of solution error in mesh size – step size convergence study: I) over resolved, II) appropriate size, and III) under resolved.

### 4.2 Richardson Extrapolation Technique as a Verification Tool

Richardson extrapolation technique was developed by Richardson (1911). Recently, Richardson extrapolation was used for code/solution verification of PDEs solvers (Karatekin, 1997; Xing and Stern, 2010) when the Method of Exact solutions (MES) is not applicable (Roache and Knupp, 1993).

The accuracy of the elastic-plastic algorithm is controlled to a large extent by the size of the strain increment. This is particularly true for the explicit algorithm, while for the implicit algorithm, size of tolerance also plays important role.

Consider for example the following experiments. Assume an initial stress at  $\sigma_0$ . Assume also that the exact stress solution is  $\sigma^*$ . To achieve this exact stress solution, a large number of small steps is applied to perform the integration. The

accuracy of the final stress  $\sigma$ , thus achieved, is controlled by the size of strain increment  $d\epsilon$ . Ideally, the final stress  $\sigma$  is accurate, that is  $\sigma \rightarrow \sigma^*$ , when  $d\epsilon \rightarrow 0$  (Lax and Richtmyer, 1956). The Taylor series expansion of  $\sigma$  with respect to  $d\epsilon$  is

$$\sigma(d\epsilon) = \sigma^* + Cd\epsilon^\beta + O(d\epsilon^{\beta+1}) \quad (7)$$

where  $C$  is constant and  $O$  is the big-O notation, which represents the higher order errors.

In Richardson Extrapolation technique, a new function is defined based on the stress integration algorithm.

$$R(d\epsilon, k) = \frac{k^\beta \sigma(d\epsilon) - \sigma(kd\epsilon)}{k^\beta - 1} \quad (8)$$

Here  $k$  is a constant that defines a number of increments that are used to create Richardson Extrapolation. For example, in the above equation,  $R(d\epsilon, k)$  is a difference between a solution ( $\sigma(d\epsilon)$ ) using single increment  $d\epsilon$ , multiplied by  $k^\beta$  and a solution ( $\sigma(kd\epsilon)$ ) obtained using  $kd\epsilon$  increment, and divided by  $k^\beta - 1$ . In addition, parameter  $\beta$  is the accuracy order that is solved for from Richardson Extrapolation tests.

Then, by substituting Eq 7 into Eq 8, we obtain

$$\begin{aligned} R(d\epsilon, k) &= \frac{k^\beta(\sigma^* + Cd\epsilon^\beta + O(d\epsilon^{\beta+1}))}{k^\beta - 1} - \frac{\sigma^* + Ck^\beta d\epsilon^\beta + O(d\epsilon^{\beta+1})}{k^\beta - 1} \\ &= \sigma^* + O(d\epsilon^{\beta+1}) \end{aligned} \quad (9)$$

Function  $R(d\epsilon, k)$  is the Richardson Extrapolation of  $\sigma(d\epsilon)$ . By comparing the final Richardson equation in Eq 9 to the original Eq 7, it is noted that the discretization error  $Cd\epsilon^\beta$  is cancelled out. It is also noted that by repeating Richardson equation one more time, one is able to cancel out the next higher order discretization error. This can be continued any number of times to cancel higher order discretization errors, however there is a tradeoff with efficiency.

The remaining problem is to determine the accuracy order parameter  $\beta$  for the elastic-plastic algorithms in Eq 7.

#### 4.3 Uncertainties in Numerical Simulation

The uncertainty of any computational simulation is defined as (ASME, 2009):

$$\delta_{simulation} = (\delta_{model} + \delta_{numerical} + \delta_{input}) - \delta_{experimental} \quad (10)$$

where  $\delta_{simulation}$  is the total uncertainty in the simulation. The terms in parenthesis in the right hand side Eq. 10 are the best effort of a numerical modeler and include:

- Modeling uncertainty,  $\delta_{model}$ ,
- Errors/uncertainties due to numerical solution schemes (iterative error, round off error, discretization error, etc)  $\delta_{numerical}$ ,
- Parametric uncertainty,  $\delta_{input}$  is the errors that propagate into the results of numerical simulation from uncertainty in input parameters, including geometry, initial/boundary conditions and material properties,

Experimental uncertainty,  $\delta_{experimental}$  is the uncertainty in the experimental measurement of the phenomena.

Reduction of each of the above-mentioned uncertainties will increase the quality of the simulation results.

Experimental uncertainty  $\delta_{experimental}$  is the problem of interest in experimental mechanics and is related to validation (Oberkampf et al., 2002b), modeling uncertainty  $\delta_{model}$  is a problem of model sophistication, and  $\delta_{input}$  is the problem of uncertain material parameters and uncertain loads, and their propagation through the system Sett et al. (2011). Thus here we only discuss the procedure to develop an upper and lower bound on the "numerical" uncertainty  $\delta_{numerical}$ .

The numerical uncertainty has its roots in the truncation error, round-off error and iterative error. First, truncation error represents the error due to solving discretized equations instead of continuum counterpart. Second, round-off error is an accumulation of errors due to finite precision calculations, machine epsilon. This error is not that important in modern computational mechanics simulations as it is usually overshadowed by other numerical errors. Finally, the iterative error is due to the limited number of iterations for solving either an algebraic system of equations or a system of discretized PDEs. The round-off errors and the iterative errors are usually considered to be smaller by orders of magnitude compared to truncation error (Oberkampf et al., 2002a; Saad, 2003).

#### 4.4 Grid Convergence Index

Grid Convergence Index (GCI) is an uncertainty quantification technique firstly used in the computational fluid dynamics (CFD) (ASME, 2009). At least three groups of incremental sizes are required to compute the GCI. The procedures of the uncertainty estimation are as follows.

- Choose three significantly different incremental sizes  $h$  and run the simulation. The increment refinement factor,  $r = h_{coarse}/h_{fine}$ , is usually greater than 1.3 based on experience (Roache, 1998b).
- Calculate the observed order  $\beta$ . Let  $h_1 < h_2 < h_3$  and  $r_{21} = h_2/h_1$ ,  $r_{32} = h_3/h_2$ .

$$\beta = \frac{\ln \left| \frac{d_{32}}{d_{21}} \right| + \varphi(\beta)}{\ln(r_{21})}$$

$$\varphi(\beta) = \ln \left( \frac{r_{21}^\beta - t}{r_{32}^\beta - t} \right) \quad (11)$$

$$t = \text{sign} \left( \frac{d_{32}}{d_{21}} \right)$$

where  $d_{32} = \omega_3 - \omega_2$ ,  $d_{21} = \omega_2 - \omega_1$  and  $\omega_n$  denotes the component of the stress result in the  $n^{th}$  incremental size.

The relative error  $e$ , as a dimensionless form, is

$$e_{21} = \left| \frac{\omega_1 - \omega_2}{\omega_1} \right|. \quad (12)$$

- The GCI is

$$GCI_{21} = \frac{Fs \cdot e_{21}}{r_{21}^\beta - 1} \quad (13)$$

where  $F_s$  is the factor of safety, and  $GCI_{21}$  represents the numerical uncertainty at the strain incremental size  $h_2$  with reference to the more accurate results at the strain incremental size  $h_1$ . Based on experience from computational fluid dynamics, a factor of safety  $F_s = 1.25$  (ASME, 2009).

It follows that the uncertainty caused by the numerical error  $U_{num}$  is equivalent to  $GCI_{21}$ . The range of uncertainty  $\pm U_{num}$  is bounding the exact mathematical solution with a 95% confidence or, in other words, it is within two standard deviations ( $\pm\sigma$ ). It is noted that notation for two standard deviations  $\pm 2\sigma$  represent the probability level (95.4%), and not the stress state.

#### 4.5 Accuracy order of Elastoplastic Algorithm

Before the implementation of Richardson Extrapolation, the accuracy order ( $\beta$ ) of the elastic-plastic algorithm needs to be determined. Both the analytical determination and the numerical estimation of accuracy order for elastic-plastic algorithms are discussed in this section. Analytical determination of accuracy order is possible for simple material models. On the other hand, for more sophisticated material models, it is only possible to develop numerical estimation of accuracy order.

##### 4.5.1 Analytical Determination of Accuracy Order

An analytical study of accuracy order for elastic perfectly plastic constitutive integration algorithms was developed by Ortiz and Popov (1985). In their study, Ortiz and Popov (1985) proved that all elastic plastic algorithms within generalized trapezoidal and generalized midpoint return mapping are at least first-order accurate. In the case of Crank-Nicolson method, where plastic corrector direction is chosen as an average of explicit (forward Euler) and implicit (backward Euler), elastic perfectly plastic constitutive integration algorithm is second order accurate.

**Remark:** Conclusions on algorithm accuracy order made by Ortiz and Popov (1985) do apply to elastic perfectly plastic material models. However, it is important to note that when material model features hardening and/or softening response (isotropic or kinematic hardening and softening) the accuracy order is unclear. In those cases, numerical estimation of the accuracy order ( $\beta$ ) is needed.

##### 4.5.2 Numerical Estimation of Accuracy Order

Another approach to determine the accuracy order is through an estimation using numerical experiments on various sizes of increments. The idea is to apply the Richardson Extrapolation on strain increment sizes. At least three different strain increment sizes are required to estimate the observed order.

Specifically, using three different strain increment sizes (a)  $d\epsilon$ , (b)  $d\epsilon/a$ , and (c)  $d\epsilon/b$ , where the scale factor  $b > a > 1.3$ , the expression of approximation of

exact solution  $\sigma^*$  is written as:

$$\begin{aligned}\sigma^* &= \frac{a^\beta \sigma\left(\frac{d\epsilon}{a}\right) - \sigma(d\epsilon)}{a^\beta - 1} + O(d\epsilon^{n+1}) \\ &= \frac{b^\beta \sigma\left(\frac{d\epsilon}{b}\right) - \sigma(d\epsilon)}{b^\beta - 1} + O(d\epsilon^{n+1})\end{aligned}\quad (14)$$

Assuming the higher order errors [ $O(d\epsilon^{n+1})$ ] are negligible we can rewrite Eq. 14 as

$$\sigma\left(\frac{d\epsilon}{a}\right) + \frac{\sigma\left(\frac{d\epsilon}{a}\right) - \sigma(d\epsilon)}{a^\beta - 1} = \sigma\left(\frac{d\epsilon}{b}\right) + \frac{\sigma\left(\frac{d\epsilon}{b}\right) - \sigma(d\epsilon)}{b^\beta - 1}\quad (15)$$

It is noted that in Eq. 15, stress solutions  $\sigma(d\epsilon)$ ,  $\sigma(d\epsilon/a)$ ,  $\sigma(d\epsilon/b)$  are measured, observed from the three numerical experiments. The only unknown in Eq. 15 is thus the accuracy order  $\beta$ , which can be easily solved for.

## 5 Elastoplastic Material Models

Elastoplastic material models used for numerical experiments are based on von Mises and hyperbolic Drucker-Prager yield surfaces. Material models of von-Mises type are used to simulate the pressure-independent material behavior. On the other hand, hyperbolic Drucker-Prager family of models are used to simulate pressure-dependent material behavior.

For modeling pressure independent behavior of material, plastic volume change is usually negligible, which leads to plastic flow directions that are perpendicular/normal to the von-Mises yield surface. This is the so called associated plasticity behavior. For modeling pressure dependent material response, plastic volume change can be significant, however plastic flow directions are usually not perpendicular/normal to the yield surface. This is the so called non-associated plasticity behavior. In addition, different types of hardening and softening of yield surface and plastic flow directions exist (Chen, 1994). For example perfectly plastic material will not feature any evolution of yield surface. On the other hand isotropic hardening and/or softening will change the yield surface size. For kinematic hardening, yield surface will move (translate or rotate) in stress space. Distortional hardening (Baltov and Sawczuk, 1965) where yield surface changes shape, is also possible, but it is rarely used. Plastic flow directions are usually developed either based on associated or non-associated, or, for more sophisticated model, directly as functions of stress and internal variable space (Dafalias and Herrmann, 1982; Lubliner, 1990; Manzari and Dafalias, 1997).

Presented below are common examples of yield surface functions for von-Mises and Drucker-Prager models, and examples of non-associated plastic flow as well as a nonlinear kinematic hardening rule.

### 5.1 The von-Mises Yield Surface

The von Mises yield surface (Lubliner, 1990), a cylinder in stress space, is given as

$$F(\sigma_{ij}, k, \alpha_{ij}) = \sqrt{\frac{3}{2}(s_{ij} - \alpha_{ij})(s_{ij} - \alpha_{ij})} - k = 0 \quad (16)$$

where  $s_{ij}$  is the deviatoric stress ( $s_{ij} = \sigma_{ij} - 1/3\sigma_{kk}\delta_{ij}$ ). The yield surface radius  $k$  is the scalar internal variable describing the size of yield surface. The back stress  $\alpha_{ij}$  represents location of yield surface in the stress space. Both yield surface radius  $k$  and the back stress  $\alpha_{ij}$  represent internal variables (generally annotated as  $q_*$ ) that can harden and/or soften.

### 5.2 Hyperbolic Drucker-Prager Yield Surface

The Drucker-Prager yield criterion is a pressure-dependent material model, where yielding of materials is controlled by the deviatoric stress, and also by the confining pressure. The original Drucker-Prager yield surface (Lubliner, 1990) has a singularity point at the location of zero deviatoric stress. Hyperbolic yield surface (Abbo and Sloan, 1995) modifies the Drucker-Prager yield surface by removing the singular point, The hyperbolic Drucker-Prager yield function is given as

$$F(\sigma, \eta, \alpha_{ij}) = \sqrt{\frac{1}{2}(s_{ij} - p\alpha_{ij})(s_{ij} - p\alpha_{ij}) + a^2\eta^2 - \eta p - \xi} \quad (17)$$

where  $\eta$  is controls the friction angle, and  $\xi$  controls the cohesion, while  $p\alpha_{ij}$  controls rotation of the yield surface. Back stress  $\alpha_{ij}$  is multiplied by mean stress  $p = \sigma_{ii}/3$  in order to force the surface to rotate. Variable  $a$  represents the rounded length between the cut-off on  $p$ -axis and the original apex points, as shown in Figure 2.

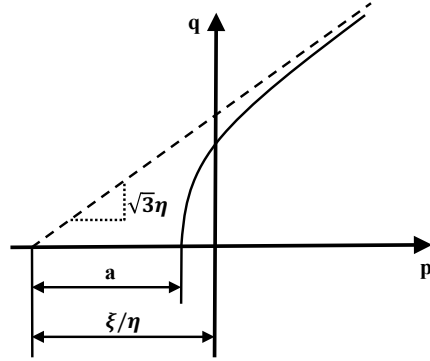


Fig. 2: The hyperbolic Drucker-Prager yield function.

### 5.3 Non-associative Plastic Flow

In pressure-dependent materials, the dilative or contractive behavior is usually not associated with the normal to the yield surface  $n_{ij} = \partial F / \partial \sigma_{ij}$ . The non-associative plastic flow direction  $m_{ij}$  is expressed as

$$m_{ij} = n_{ij} - \frac{1}{3} D \delta_{ij} \quad (18)$$

where dilatancy parameter  $D$  is defined as

$$D = \zeta \left( \sqrt{\frac{2}{3}} k_d - \frac{\sqrt{s_{mn}s_{mn}}}{p} \right) \quad (19)$$

The volumetric plastic strain rate  $\zeta$  governs the amplitude of plastic volume changes. The term  $\sqrt{s_{mn}s_{mn}}/p$  represents the stress-ratio. The material constants  $k_d$  governs the critical stress-ratio, which controls the direction of the plastic flow. The dilative or contractive behavior is controlled by the stress-ratio ( $\sqrt{s_{mn}s_{mn}}/p$ ) (Muir Wood, 1990). When dilatancy parameter  $D < 0$  plastic compaction takes place, whereas when dilatancy parameter  $D > 0$  plastic dilatancy takes place.

### 5.4 Armstrong-Frederick Hardening Law

Nonlinear kinematic hardening law developed by Armstrong and Frederick (1966) simulates nonlinear behavior of materials through control of the back stress ( $\alpha_{ij}$ )

$$d\alpha_{ij} = \frac{2}{3} h_a (d\epsilon_{ij}^p)^{dev} - c_r \alpha_{ij} \sqrt{\frac{2}{3} (d\epsilon_{rs}^p)^{dev} (d\epsilon_{rs}^p)^{dev}} \quad (20)$$

where  $d\alpha_{ij}$  is increment of the back-stress,  $h_a$  is the initial rate of change of back-stress,  $h_a/c_r$  controls the limit, asymptote of the back-stress, and  $(d\epsilon_{ij}^p)^{dev}$  is the deviatoric component of increment of plastic strain.

## 6 Error Maps for Elastoplastic Constitutive Integration

Verification examples in Sections 6.1, 6.2, and 6.3 present error maps in octahedral stress plane, for different stress step size, different constitutive integration algorithms, for von-Mises elastic perfectly plastic material model. Next two examples, Sections 6.4, and 6.5 quantitatively evaluated the accuracy of forward and backward Euler algorithms for linear kinematic hardening, associated and non-associated hyperbolic Drucker-Prager material model.

In the error maps, the relative stress norm  $\delta_{norm}$  is defined as

$$\delta_{norm} = \frac{\|\sigma_{ij} - \sigma_{ij}^{exact}\|}{\|\sigma_{ij}^{exact}\|} \quad (21)$$

where stress  $\sigma_{ij}$  is the calculated stress result, and stress  $\sigma_{ij}^{exact}$  is the exact stress from either analytical solutions or Richardson extrapolation.

### 6.1 Error Map for von-Mises Perfectly Plastic Material Model

In this section, the von-Mises perfectly plastic material model is verified by the prescribed solutions forcing (PSF) method. This type of material uses the radial return algorithm, (Krieg and Krieg, 1977; Lubarda and Benson, 2002).

At the beginning of the verification test, the current stress state is set on the yield surface at the Lode angle  $\theta = -30^\circ$ . Different elastic predictors are applied to this initial stress state. The explicit, forward Euler constitutive integration algorithm solve the problem exactly for radial stress predictors as solution consists of an exact radial return. This is observed in zero error Figure 3, However, when the direction of the elastic predictors deviates far from the normal to the yield surface, radial direction, explicit, forward Euler constitutive integration algorithm creates an error. That error increases as the predictor stress increases, as observed in Figure 3.

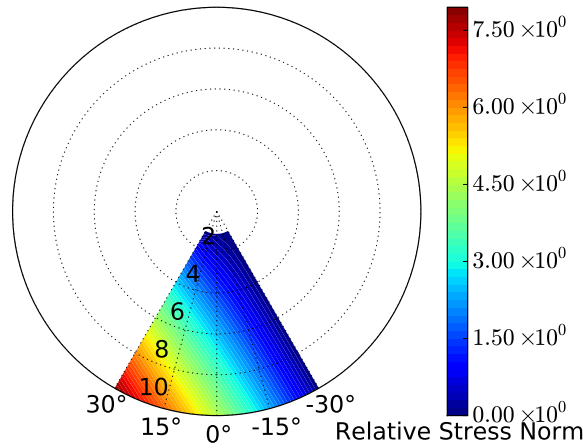


Fig. 3: Relative stress norm of von-Mises perfectly plastic material model with the forward Euler algorithm.

The explicit, forward Euler constitutive integration algorithm together with sub-incrementation technique, using 100 sub-incrementation, is able to reduce the numerical errors and return the stress states more accurately to the yield surface, as shown in Figure 4. However, sub-incrementation does require much more time, so benefits of accuracy increase have to be balanced with more time required for simulation.

For implicit, backward Euler constitutive integration algorithm, accuracy is prescribed by the analyst as a yield function and/or residual stress tolerance. The numerical errors for the of implicit, backward Euler constitutive integration algorithm are shown in Figure 5.

By comparing error maps shown in Figs. 3, 4, and 5, it is obvious that backward Euler algorithm achieves the highest accuracy, by far. However, back-

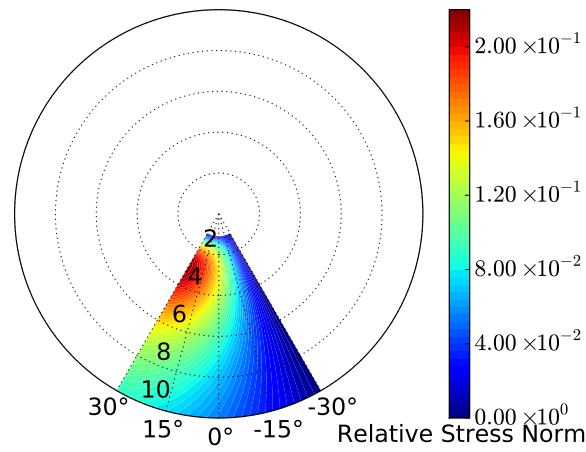


Fig. 4: Relative stress norm of von-Mises perfectly plastic material model with *sub-increment technique*, which reduces the relative stress error.

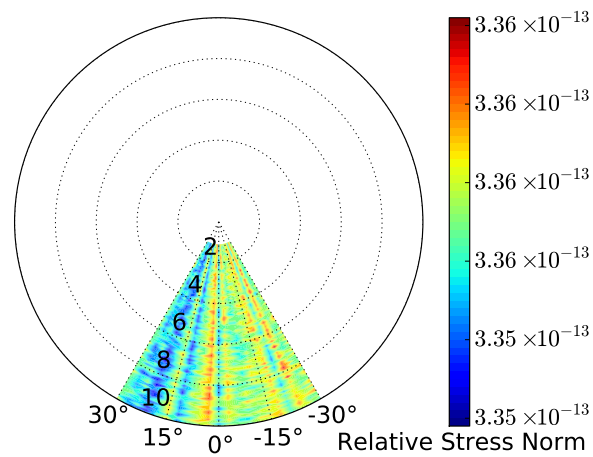


Fig. 5: Relative stress norm of von-Mises perfectly plastic material model with *backward Euler* algorithm, which achieves accurate stress results.

ward Euler constitutive integration algorithm incurs high computational costs, as higher order derivatives of plastic flow directions and equilibrium iterations are needed. Forward Euler algorithm is rather simple and fast algorithm that can be alternatively used, perhaps with the sub-incrementation option to solve problems.

## 6.2 Error Map for Hyperbolic Drucker-Prager Linear Kinematic Hardening Material Model

For linear hardening, modified hyperbolic Drucker-Prager material model, exact solution does not exist. Linear kinematic hardening simplifies solution, however the nonlinear part of the modified Drucker-Prager yield surface adds additional nonlinearities that introduce error in constitutive integrations. In this case Richardson extrapolation is used to verify the constitutive integration algorithms. Richardson extrapolation provides means to obtain accurate results that are then used for error calculations. Accurate results are developed using Richardson extrapolation and three groups of tests, in order to determine accuracy order.

- Test 1. The elastic predictor is applied in 1 increment.
- Test 2. The elastic predictor is applied in 10 sub-incrementation, where the total magnitude of 10 sub-incrementation is the same as the 1 elastic predictor in Test 1.
- Test 3. The elastic predictor is applied in 100 sub-incrementation, where the total magnitude of 100 sub-incrementation is the same as the 1 elastic predictor in Test 1.

Results from these numerical experiments are then used to calculate the accuracy order using Equation (15). With calculated accuracy order, accurate solution can be developed, and then used in calculating errors for different algorithms, as shown below.

Figure (6) shows results for explicit, forward Euler constitutive integration algorithm, applied to linear hardening, modified hyperbolic Drucker-Prager material model.

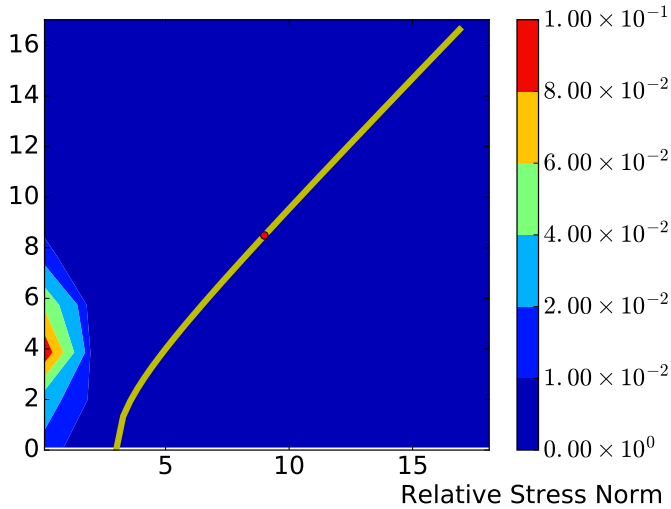


Fig. 6: Error map of explicit algorithms for hyperbolic Drucker-Prager linear kinematic hardening material model.

It is noted that error maps, as show in Figure (6), are presented in deviatoric stress plane, where horizontal axes represents mean stress ( $p = -(1/3)\sigma_{ii}$ ), and vertical axes represents shear stress invariant ( $q = \sqrt{(3/2)s_{ij}s_{ji}}$ ) and stress deviator  $s_{ij}$  is defined as  $s_{ij} = \sigma_{ij} - (1/3)\delta_{ij}\sigma_{kk}$ , and  $\delta_{ij}$  is the Kronecker delta. It is noted that starting point is at the location of  $p = 8\text{kPa}$  and  $q = 8\text{kPa}$ , and is marked with a red dot. Error map for explicit constitutive integration algorithm, shown in Figure 6 reveals a potentially problematic stress region on the tensile side of the yield surface. However, it is noted that regular Drucker-Prager yield surface would not be even able to produce results for this side of stress space, as yield surface derivatives are not even defined in that region.

Figure 7 show results for the implicit, backward Euler constitutive integration algorithm, applied to linear hardening, modified hyperbolic Drucker-Prager material model. It is noted that errors are much smaller than for explicit algorithm. It

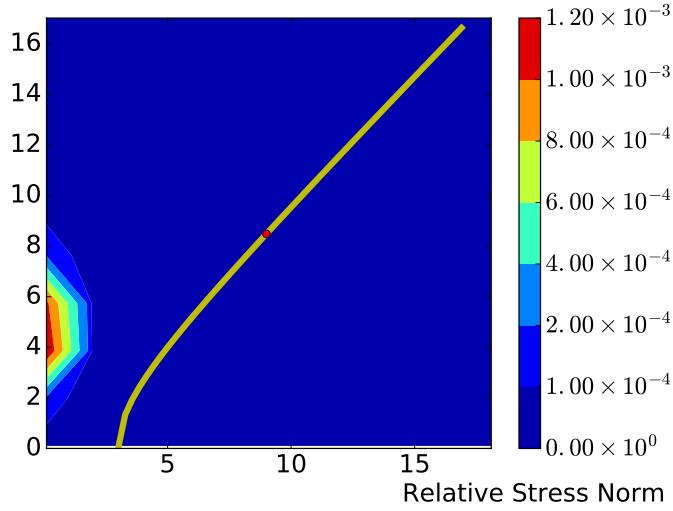


Fig. 7: Error map of implicit algorithms for hyperbolic Drucker-Prager linear kinematic hardening material model.

is also noted that tensile region still tends to introduce more error, however errors are still much smaller than with the explicit algorithm.

### 6.3 Error Map for Hyperbolic Drucker-Prager Armstrong-Frederick Nonlinear Kinematic Hardening Material Model

More advanced material models used in elastoplastic modeling of cyclic behavior feature nonlinear kinematic hardening. It is thus important to verify constitutive integration for the nonlinear kinematic hardening material models. In this section, Richardson Extrapolation technique is used to verify constitutive integration of nonlinear kinematic hardening material model. Material model used here is based on the Armstrong-Frederick nonlinear kinematic hardening function (Armstrong and Frederick, 1966). Using similar approach for estimating accuracy order as in Section 6.2, and the Richardson Extrapolation algorithm, the error map for constitutive integration of elastoplastic material with Armstrong-Frederick nonlinear kinematic hardening law is shown in Figures. 8 and 9

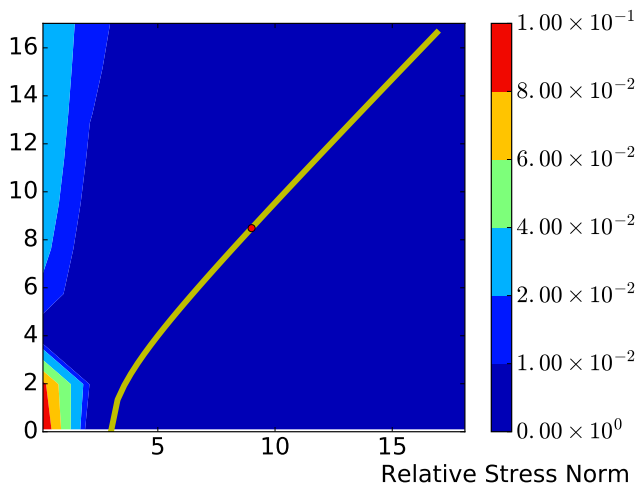


Fig. 8: Error map of explicit algorithms for hyperbolic Drucker-Prager nonlinear kinematic hardening material model.

A number of observations can be made.

- The errors using implicit constitutive integration is much smaller than that using explicit constitutive integration. It is noted that the error in implicit algorithm is at least two orders of magnitude smaller than the error in explicit algorithm, as seen in Figures 8 and 9.
- Comparison of errors for explicit constitutive algorithm for linear and nonlinear kinematic hardening models, Figures 6 and 8 , reveals that nonlinearity in hardening did introduce additional error, as expected.
- However, comparison of errors for implicit constitutive algorithm for linear and nonlinear kinematic hardening models, Figures 7 and 9 reveals very similar error distribution. This is also expected as for the implicit algorithm convergence tolerance is prescribed and it holds for any material model used.

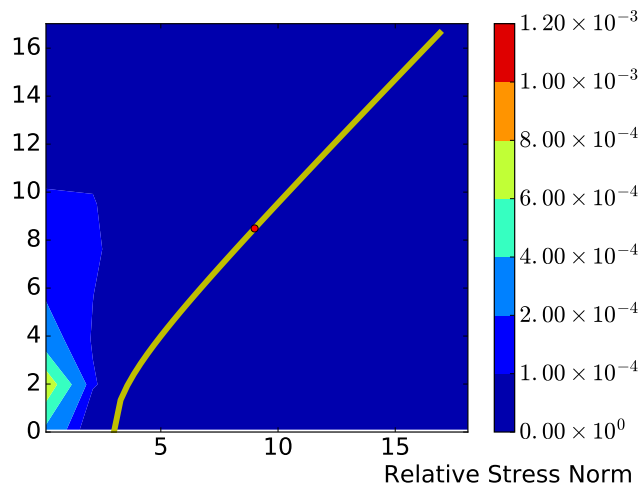


Fig. 9: Error map of implicit algorithms for hyperbolic Drucker-Prager nonlinear kinematic hardening material model.

- Constitutive integration error for both implicit and explicit algorithms increases as the mean pressure is decreases, that is, as the stress states is closer to the nonlinear part of the yield surface.

#### 6.4 Numerical Accuracy Estimation for Associated Drucker-Prager Linear Kinematic Hardening Material Model

Presented in this section are estimates of numerical accuracy of constitutive integration for a Drucker-Prager material model with linear kinematic hardening. Three groups of tests are conducted using Drucker-Prager associative material model. For each of numerical experiments, the total strain increment is the same, however, the number of increments to reach this strain are different. This means that the size of strain sub-increments for each test differs. Table 1 presents results of Richardson extrapolation for three different starting stress point on the Drucker-Prager yield surface, and corresponds to three confining pressures ( $p = 10^4\text{Pa}; 10^5\text{Pa}; 10^6\text{Pa}$ ).

Table 1: Richardson extrapolation results for shear stress  $q$  for Drucker-Prager linear kinematic hardening material with different confinements.

Confinement	$10^4\text{Pa}$	$10^5\text{Pa}$	$10^6\text{Pa}$
Accuracy order $\beta$	1.0003	1.0017	0.9954
GCI	0.01%	0.01%	0.00%
Resulting $q$	32207.705Pa	41866.802Pa	127602.165Pa
Richardson exact result for $q$	32205.934Pa	41864.904Pa	127600.876Pa
Range of error in $q$	$\pm 2.213\text{Pa}$	$\pm 2.373\text{Pa}$	$\pm 1.611\text{Pa}$

Figure 10, shows results for asymptotic convergence of Drucker-Prager associative linear kinematic hardening material model with different starting points (different confinement levels).

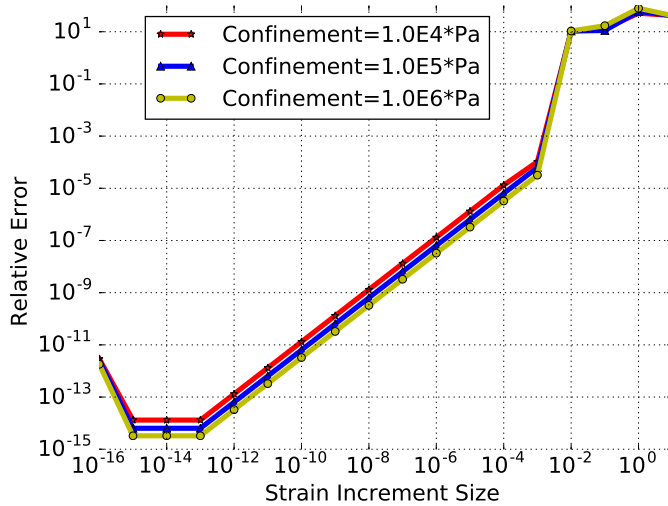


Fig. 10: Asymptotic convergence of Drucker-Prager linear kinematic hardening material with different confinements using implicit, backward Euler algorithm.

Based on Figure 10, A number of observations can be made:

- When the strain increment size is greater than  $1e-3$ , the relative error oscillates since the discretization size is too large to represent the actual continua space in the discretized domain.
- When the strain increment size is between  $1e-13$  and  $1e-3$ , the relative error decreases asymptotically. This region is called the asymptotic regime of convergence.
- When the strain increment size is smaller than  $1e-13$ , the relative error cannot decrease anymore since round-off error contributes to the solution error.
- When the strain increment is  $1e-16$  (less than the machine epsilon  $2.22e-16$ ), the stress result oscillates significantly since the round-off error dominates the solution error.

Besides, the relative error decreases when the confining pressure increases. This is due to the fact that high pressure states of stress are far from the nonlinearities in the modified hyperbolic function. This nonlinearity leads to increase in integration error, while moving away from such nonlinearity decreases of the relative error.

### 6.5 Numerical Accuracy Estimation for Non-Associated Drucker-Prager Nonlinear Kinematic Hardening Material Model

In this section, a non-associated Drucker-Prager material model with nonlinear, Armstrong-Frederick kinematic hardening is investigated. Both explicit, forward Euler and implicit, backward Euler algorithms are tested with various strain incremental sizes. Stress solution, in terms of deviatoric stress ( $q = \sqrt{3/2}s_{ij}s_{ji}$ ,  $s_{ij} = \sigma_{ij} - \sigma_m\delta_{ij}$ ) is used to illustrate change of accuracy of algorithms for various incremental step sizes. Figure 11 shows the comparison of deviatoric stress solution for a variation in incremental strain size for implicit and explicit algorithms.

It is noted that implicit algorithm behaves as expected, that is stress solution is very accurate even for large strain increments, while explicit algorithm does produce significant error for larger step sizes. For explicit algorithm, error is significantly reduced when the step size becomes small. This argument is used for advocating sub-stepping approach in order to improve explicit algorithm accuracy.

In addition to stress result, yield surface values of the stress results are also used to illustrate numerical accuracy of the algorithms. Ideally, constitutive integration algorithm should return the stress state to the yield surface, yielding yield surface values to (almost) zero. If stress is not returned to the yield surface, equilibrium of internal stress and external forces might not be achievable. In addition, calibration of the elastic-plastic material model is done assuming that stress state is on the yield surface during plastification. If stress state is not on the yield surface, then the calibrated parameters for material model will not be able to replicate real response.

Figure 12, shows yield surface values for both implicit and explicit algorithms for different incremental step sizes.

It is noted that, as expected, for explicit algorithm, stress solutions drifts away from the yield surface for larger incremental step sizes, hence producing erroneous stress solution with calibrated material parameters. On the other hand, implicit

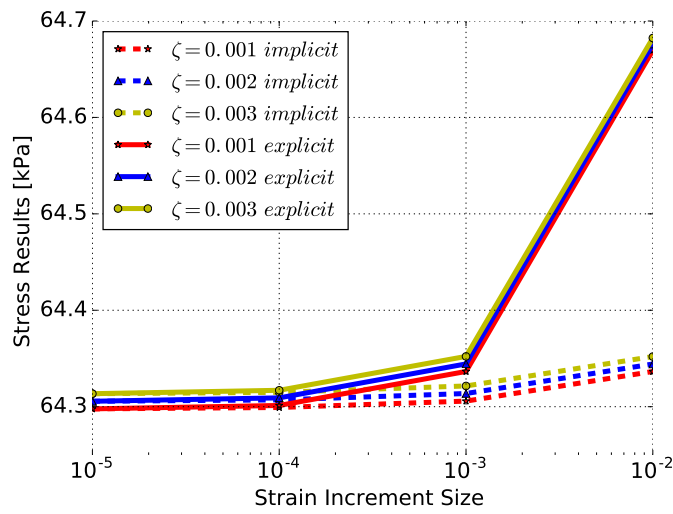


Fig. 11: Deviatoric Stress  $q$  results for a non-associative Drucker-Prager nonlinear kinemastic hardening material using implicit, backward Euler and explicit, forward Euler algorithms.

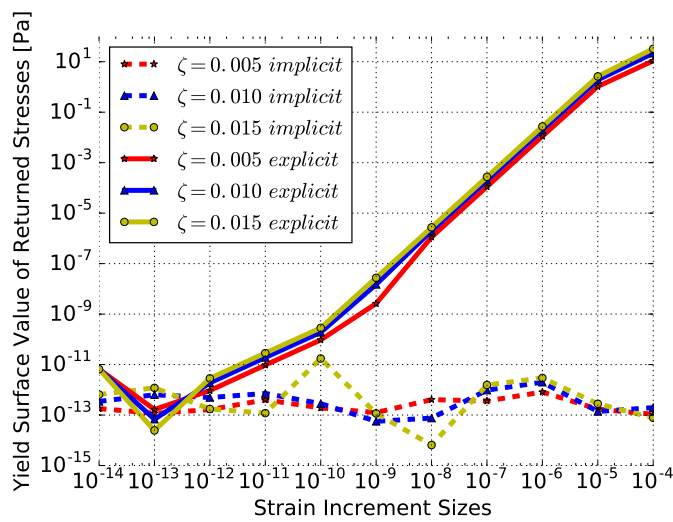


Fig. 12: Yield surface values of returned stress of non-associative plastic material using implicit, backward Euler and explicit, forward Euler algorithms.

algorithm performs much better, since user controls stress solution drift from the yield surface by prescribing drift tolerance.

While explicit integration algorithm is simpler to develop and implement than the explicit integration algorithm, it does produce larger error for realistic incremental strain steps. Use of sub-incrementation is possible at a cost of increasing computational times. On the other hand, implicit integration algorithm is more complicated and requires iterations, thus increasing computational time, however, accuracy is superior.

## 7 Conclusion and Final Remarks

This paper deals with verification of constitutive integration algorithms as applied to elastic-plastic materials models used in civil engineering. Both explicit, forward Euler and implicit, backward Euler elastoplastic algorithms are verified on the constitutive level. Three methods are used in the verification process, including the prescribed solution forcing, Richardson extrapolation, and the extension grid convergence index (GCI).

In the particular case of elastic-plastic constitutive integrations, verification was performed using:

1. Prescribed solution forcing in terms of analytical solutions, to verify the perfectly plastic material with a hyperbolic Drucker-Prager yield surface.
2. Richardson extrapolation, to verify the nonlinear kinematic hardening material models.
3. GCI method, to estimate the numerical accuracy in the elastoplastic algorithm, especially for Drucker-Prager material models with non-associate plastic flow.

It was shown that constitutive algorithms that were subject to verification perform well and as expected, thus increasing confidence in elastic plastic modeling.

It is also important to note that use of numerical modeling for prediction of behavior of solids and structures has to be done using verified numerical tools. This is rarely demonstrated in project documentation and scientific publications, which lowers confidence in presented results.

### Acknowledgements

Funding from the United States Department of Energy is acknowledged.

### References

- A. Abbo and S. Sloan. A smooth hyperbolic approximation to the mohr-coulomb yield criterion. *Computers and Structures*, 54(3):427 – 441, 1995. ISSN 0045-7949. doi: [http://dx.doi.org/10.1016/0045-7949\(94\)00339-5](http://dx.doi.org/10.1016/0045-7949(94)00339-5). URL [//www.sciencedirect.com/science/article/pii/0045794994003395](http://www.sciencedirect.com/science/article/pii/0045794994003395).
- P. Armstrong and C. Frederick. A mathematical representation of the multiaxial bauschinger effect. Technical Report RD/B/N/ 731,, C.E.G.B., 1966.
- V. C. ASME. Standard for verification and validation in computational fluid dynamics and heat transfer. *American Society of Mechanical Engineers, New York*, 2009.

- I. Babuška and J. T. Oden. Verification and validation in computational engineering and science: basic concepts. *Computer Methods in Applied Mechanics and Engineering*, 193(36-38):4057–4066, Sept 2004.
- A. Baltov and A. Sawczuk. A rule of anisotropic hardening. *Acta Mechanica*, I (2):81–92, 1965.
- W. Chen. *Constitutive Equations for Engineering Materials: Plasticity and Modeling*, volume 2 of *Studies in applied mechanics 37B*. Elsevier, ELSEVIER SCIENCE B.V. Sara Burgerharstraat 25, P.O.Box 211, 1000 AE Amsterdam, The Netherlands, 1994. In collaboration with W. O. McCarron, AMOCO production Company, Tulsa, OK, USA and E. Yamaguchi, University of Tokyo, Japan.
- M. A. Crisfield. *Non-Linear Finite Element Analysis of Solids and Structures Volume 1: Essentials*. John Wiley and Sons, Inc. New York, 605 Third Avenue, New York, NY 10158-0012, USA, 1991.
- M. A. Crisfield. *Non-Linear Finite Element Analysis of Solids and Structures Volume 2: Advanced Topics*. John Wiley and Sons, Inc. New York, 605 Third Avenue, New York, NY 10158-0012, USA, 1997.
- Y. F. Dafalis and L. R. Herrmann. Bounding surface formulation of soil plasticity. In G. N. Pande and O. C. Zienkiewicz, editors, *Soil Mechanics – Transient and Cyclic Loads*, pages 253–282. John Wiley and Sons Ltd., 1982.
- D. P. Dee. Prescribed solution forcing method for model verification. In *Hydraulic Engineering, Proc. 1991 National Conf. of Hydr. Engrg*, pages 734–739. Citeseer, 1991.
- D. C. Drucker and W. Prager. Soil mechanics and plastic analysis or limit design. *Quarterly of applied mathematics*, 10(2):157–165, 1952.
- M. Grottke and K. S. Trivedi. Fighting bugs: Remove, retry, replicate, and rejuvenate. *Computer*, 40(2), 2007.
- L. Hatton. The T experiments: Errors in scientific software. *IEEE Computational Science and Engineering*, 4(2):27–38, April–June 1997.
- L. Hatton and A. Roberts. How accurate is scientific software? *IEEE Transaction on Software Engineering*, 20(10):185–797, October 1994.
- D. Ingraham and R. Hixon. External verification analysis: A code-independent verification technique for unsteady pde codes. *Journal of Computational Physics*, 243:46–57, 2013.
- J.-M. Jazequel and B. Meyer. Design by contract: The lessons of ariane. *Computer*, 30(1):129–130, 1997.
- B. Jeremić. Implicit integration rules in plasticity: Theory and implementation. Master’s thesis, University of Colorado at Boulder, May 1994.
- K. Kamojjala, R. Brannon, A. Sadeghirad, and J. Guilkey. Verification tests in solid mechanics. *Engineering with Computers*, 29(4), November 2013.
- O. Karatekin. Numerical experiments on application of Richardson extrapolation with nonuniform grids. *Journal of Fluids Engineering*, 1997.
- R. D. Krieg and D. B. Krieg. Accuracies of numerical solution methods for the elastic - perfectly plastic model. *Journal of Pressure Vessel Technology*, pages 510–515, November 1977.
- P. D. Lax and R. D. Richtmyer. Survey of the stability of linear finite difference equations. *Communications on pure and applied mathematics*, 9(2):267–293, 1956.
- V. A. Lubarda and D. J. Benson. On the numerical algorithm for isotropic-kinematic hardening with the Armstrong-Frederick evolution of the back stress.

- Comput. Methods Appl. Mech. Eng.*, 191(33):3583–3596, 2002. ISSN 00457825. doi: 10.1016/S0045-7825(02)00296-7.
- J. Lubliner. *Plasticity Theory*. Macmillan Publishing Company, New York., 1990.
- M. T. Manzari and Y. F. Dafalias. A critical state two–surface plasticity model for sands. *Géotechnique*, 47(2):255–272, 1997.
- G. E. Moore. Cramping more components onto integrated circuits. *Electronics Magazine*, 38(8), April 1965.
- D. Muir Wood. *Soil Behaviour and Critical State Soil Mechanics*. Cambridge University Press, 1990.
- W. L. Oberkampf and C. J. Roy. *Verification and Validation in Scientific Computing*. Cambridge University Press, 2010. ISBN 978-0-521-11360-1.
- W. L. Oberkampf, S. M. DeLand, B. M. Rutherford, K. V. Diegert, and K. F. Alvin. Error and uncertainty in modeling and simulation. *Reliability Engineering & System Safety*, 75(3):333–357, 2002a.
- W. L. Oberkampf, T. G. Trucano, and C. Hirsch. Verification, validation and predictive capability in computational engineering and physics. In *Proceedings of the Foundations for Verification and Validation on the 21st Century Workshop*, pages 1–74, Laurel, Maryland, October 22-23 2002b. Johns Hopkins University / Applied Physics Laboratory.
- J. T. Oden, I. Babuška, F. Nobile, Y. Feng, and R. Tempone. Theory and methodology for estimation and control of errors due to modeling, approximation, and uncertainty. *Computer Methods in Applied Mechanics and Engineering*, 194(2-5):195–204, February 2005.
- T. Oden, R. Moser, and O. Ghattas. Computer predictions with quantified uncertainty, part i. *SIAM News.*, 43(9), November 2010a.
- T. Oden, R. Moser, and O. Ghattas. Computer predictions with quantified uncertainty, part ii. *SIAM News.*, 43(10), December 2010b.
- M. Ortiz and E. P. Popov. Accuracy and stability of integration algorithms for elastoplastic constitutive relations. *International Journal for Numerical Methods in Engineering*, 21:1561–1576, 1985.
- L. F. Richardson. The approximate arithmetical solution by finite differences of physical problems involving differential equations, with an application to the stresses in a masonry dam. *Philosophical Transactions of the Royal Society of London. Series A, Containing Papers of a Mathematical or Physical Character*, 210:307–357, 1911.
- P. J. Roache. Quantification of uncertainty in computational fluid dynamics. *Annual review of fluid Mechanics*, 29(1):123–160, 1997.
- P. J. Roache. *Verification and Validation in Computational Science and Engineering*. Hermosa Publishers, Albuquerque, New Mexico, 1998a. ISBN 0-913478-08-3.
- P. J. Roache. Verification of codes and calculations. *AIAA journal*, 36(5):696–702, 1998b. URL <http://arc.aiaa.org/doi/pdf/10.2514/2.457>.
- P. J. Roache. Code verification by the method of manufactured solutions. *Journal of Fluids Engineering*, 124(1):4–10, 2002. URL <http://www.osti.gov/scitech/servlets/purl/759450/>.
- P. J. Roache and P. M. Knupp. Completed Richardson extrapolation. *International Journal for Numerical Methods in Biomedical Engineering*, 9(5):365–374, 1993.
- C. J. Roy and W. L. Oberkampf. A comprehensive framework for verification, validation, and uncertainty quantification in scientific computing. *Computer Meth-*

